Wei et al. Nanoscale Research Letters (2018) 13:227
https://doi.org/10.1186/s11671-018-2640-0

Nanoscale Research Letters

NANO EXPRESS Open Access

Channel Plasmon Nanowire Lasers with V-Groove Cavities

Wei Wei[1*], Xin Yan[2], Bing Shen[3], Jian Qin[1] and Xia Zhang[2]

Abstract

A hybrid channel plasmon nanowire laser based on GaAs/AlGaAs core-shell semiconductor nanowire and silver V-groove is proposed. The laser structure has potential capability of integrating with plasmonic waveguides, using channel plasmon-polariton modes in V-groove plasmonic waveguides. Guiding and lasing properties are numerically calculated using finite elements method. From the theoretical results, the laser could support guiding mode with a smallest diameter of 40 nm. Lasing emission could happen at a relatively low threshold around 2000 cm^{-1} when the diameter is larger than 140 nm. A quite large Purcell factor of 180 could be achieved to enhance the spontaneous emission rate.

Keywords: Channel plasmon-polariton, Nanowire, Nanolaser

Background

With cylindrical geometry and strong two-dimensional confinement of electrons, holes, and photons, independent semiconductor nanowire is ideal for semiconductor laser with reduced threshold and compact size [1–6]. Up to date, room-temperature lasing emission has been realized in ZnO, GaN, CdS, and GaAs nanowires, covering optical spectrum from ultra-violet to near-infrared [7–12]. To continue shrinking dimensions of nanowires beyond the diffraction limit, plasmonic nanowire lasers has been proposed and experimentally demonstrated, including hybrid plasmonic nanowire lasers and high-order mode plasmon nanowire lasers [13–15]. Among them, hybrid plasmonic nanowire lasers achieved much smaller dimension limit. Recently, plasmonic nanowire laser showed its capability of integrating with plasmonic waveguides, using channel plasmon-polariton (CPP) modes in V-groove plasmonic waveguides [16]. The diameters adopted in the experiment are above 300 nm. CPPs are the plasmon polaritons guided by a V-shaped groove carved in metal, which was first theoretically suggested by Maradudin and co-workers [17]. CPPs showed strong confinement, low damping, and robustness against channel bending at near-infrared wavelengths [18–20].

Here, by combining the low dissipation of hybrid plasmonic modes with the strong confinement and integration with plasmonic waveguides of CPP mode, we propose a hybrid channel plasmon nanowire (CPN) lasers and numerically investigate the modal and lasing properties. The CPN laser is comprised of a core-shell GaAs/AlGaAs nanowire and silver V-groove which is separated by an ultra-thin dielectric layer of MgF_2, in which the diameter of nanowire locates in the range of 40 to 220 nm to explore the lasing properties beyond the diffraction limit. Due to the hexagonal shape of GaAs/AlGaAs nanowire, two integrated structures of CPN lasers will be shown in next section.

PPN Laser Structures

The schematic of the CPN laser structures are demonstrated in Fig. 1, where the background material is air, the material in gray is silver, whose permittivity is described by the Drude model $\varepsilon_r = \varepsilon_\infty - \omega_p^2/(\omega^2 + j\gamma\omega)$, with ε_∞=3.7, ω_p=9.1 eV, and γ=0.018 eV [21]. The nanowire laying in the V-groove has a core-shell structure, the core material is GaAs and the shell material is AlGaAs. The GaAs core is passivated by a thin AlGaAs shell layer of 10 nm to improve radiative efficiency [12]. Between the nanowire and V-groove is an ultrathin dielectric layer of MgF_2. Its thickness is fixed at 5 nm to support low-loss propagation under strong optical confinement. There are two integration ways of CPN lasers. The first one we call it CPN-N

* Correspondence: wei.wei@outlook.ie
[1]School of Mechanical and Electric Engineering, Guangzhou University, Guangzhou 510006, China
Full list of author information is available at the end of the article

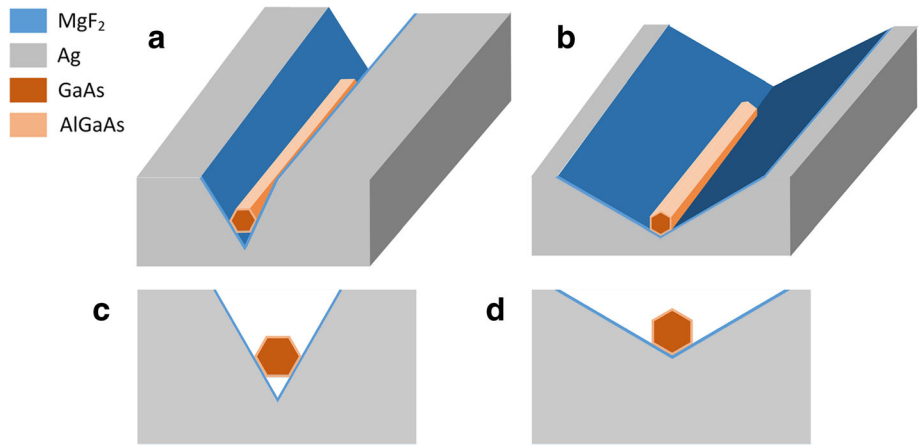

Fig. 1 Schematic diagram of the CPN laser structures. **a** CPN-N. **b** CPN-W. **c** Cross-section of CPN-N. **d** Cross-section of CPN-W

(CPN-narrow-angle) as shown in Fig. 1a, c, where the nanowire horizontally lays on the surface of V-groove with a narrow angle of 60°. The nanowire has two sides contact with dielectric layer and the V-groove surface, between the bottom side and the vertex of V-groove is air. The second one we call it CPN-W (CPN-wide-angle) as shown in Fig. 1b, d, where the nanowire vertically lays on the surface of V-groove with a wide angle of 120°. The nanowire has not only two sides contact but also a vertex contact with the dielectric layer and the V-groove surface.

Supported CPP modes in the V-groove depend on the angle and depth of the groove, especially the angle. Normally, the number of CPP modes supported by the groove decreases with the increasing angles, and in a finitely deep groove, no CPP can exist in the groove if the degree is larger than the critical degree [22]. Strong localization of CPP can be achieved in grooves with sufficiently small angles [23], which is also shown in Fig. 2. In Fig. 2a–c, the depth of groove is fixed at 1 μm, the angles of groove are 10°, 30°, and 60°, respectively. Electric field is strongly localized in the bottom of the groove with 10°, forming CPP mode. Whereas, electric field begins to distribute towards the edge of the groove with 30°, indicating the localization becomes much weaker. With the increased angle of groove to 60°, no CPP exist the groove. However, as shown in Fig. 2d, e, with the integration of nanowire, CPP still exist in wide angle of 60° and 120° (depth is smaller than 1 μm) and tightly localized inside the low-dielectric MgF_2 layer, which is totally different from normal grooves. In a hybrid plasmonic structure like CPN cavity, the coupling between dielectric and plasmonic modes across the ultrathin dielectric layer enables 'capacitor-like' energy storage that allows subwavelength light propagation in non-metallic regions with nanolocalized electromagnetic field [24]. So, the electric field of CPP is strongly localized in the MgF_2 gap between the nanowire and groove, even in the groove with wide angles. Further guiding and lasing properties in CPN-N and CPN-W lasers will be elaborated in next section.

Results and Discussion

With the advantage of hybrid plasmonic modes, electric field can be localized in dimensions beyond the diffraction limit with low-loss propagation [25, 26]. So, our investigation focuses on the guiding and lasing properties in subwavelength diameter dimension, 40 to 220 nm. Although it is challenging to precisely control the position of nanowire with diameter below 100 nm, more or less ideal condition is considered here to explore the potential performance of CPN lasers.

Like other plasmonic nanowire lasers, more guided modes are supported in CPN lasers with the increasing diameters of nanowires. As shown in Fig. 3, the nanowire with a diameter of 200 nm incorporated in the groove can support four guided modes, HE_{11x}, HE_{11y}, TE_{01}, and TM_{01}. The surface of groove is parallel to the sides of nanowire, so the groove angle keeps invariable as the nanowire diameter changes. In a plasmonic nanowire laser with planar substrate, the nanowire has only one side contact with the substrate, leading to the coupling only between photonic modes of HE_{11y} and surface plasmons. Whereas, in a CPN structure, both HE_{11x} and HE_{11y} couple with surface plasmons forming hybrid channel plasmonic modes due to two sides contact between the nanowire and the surface of groove. For modes TE_{01} and TM_{01}, electromagnetic energy inside the nanowire also couples with the surface plasmons on the groove surface forming channel plasmonic modes. The above four modes are the guided modes in CPN lasers with diameter of 200 nm, and modes cut off with the decreasing diameter.

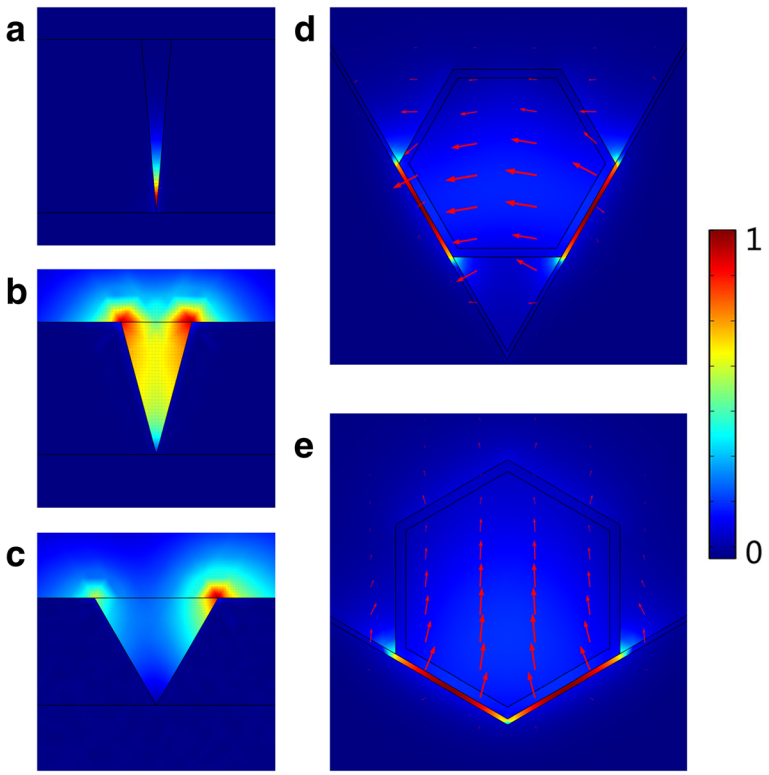

Fig. 2 Electric field distribution in **a** groove with 10°. **b** Groove with 30°. **c** Groove with 60°. **d** CPN-N laser. **e** CPN-W laser. The red arrows indicate the orientation of electric field

To investigate the guiding and lasing properties of the CPN laser, dependences of the real part of effective index, modal loss, modal confinement factor, and threshold gain on the nanowire diameter D are calculated and presented in Fig. 4a–d. Modes HE_{11x}, HE_{11y}, TE_{01}, and TM_{01} of CPN-N and CPN-W lasers are all investigated here. Properties of CPN-N and CPN-W lasers are marked as block symbol with solid line and circle symbol with dashed line, respectively. It is worth to note that the groove depth here is much larger than the nanowire diameter to eliminate the influence of the groove edge. As shown in Fig. 4a, there is a positive correlation between the real part of the effective indices $\mathrm{Re}(n_{\mathrm{eff}})$ and nanowire diameter D. This behaves the same as the effective index of an individual nanowire. With the increasing diameter of nanowire, the equivalent index of the structure becomes larger, leading to the increasing modal index. As the diameter decreases, mode

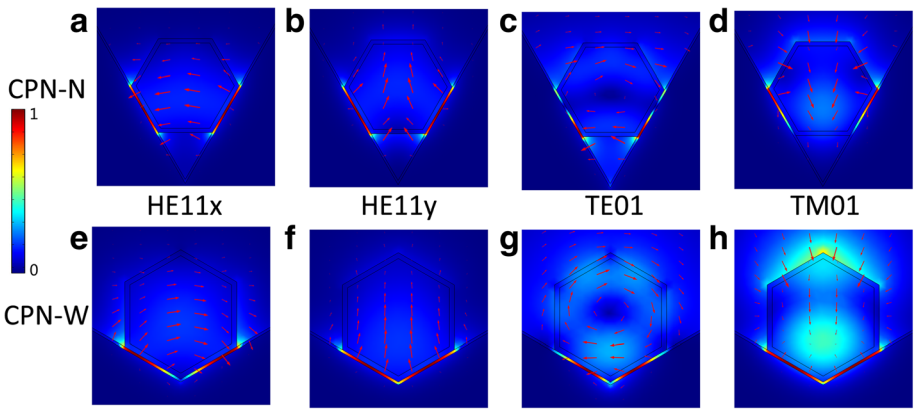

Fig. 3 Electric field distribution of modes in CPN-N laser (**a**–**d**) and CPN-W laser (**e**–**h**). Nanowire diameter is fixed at 200 nm

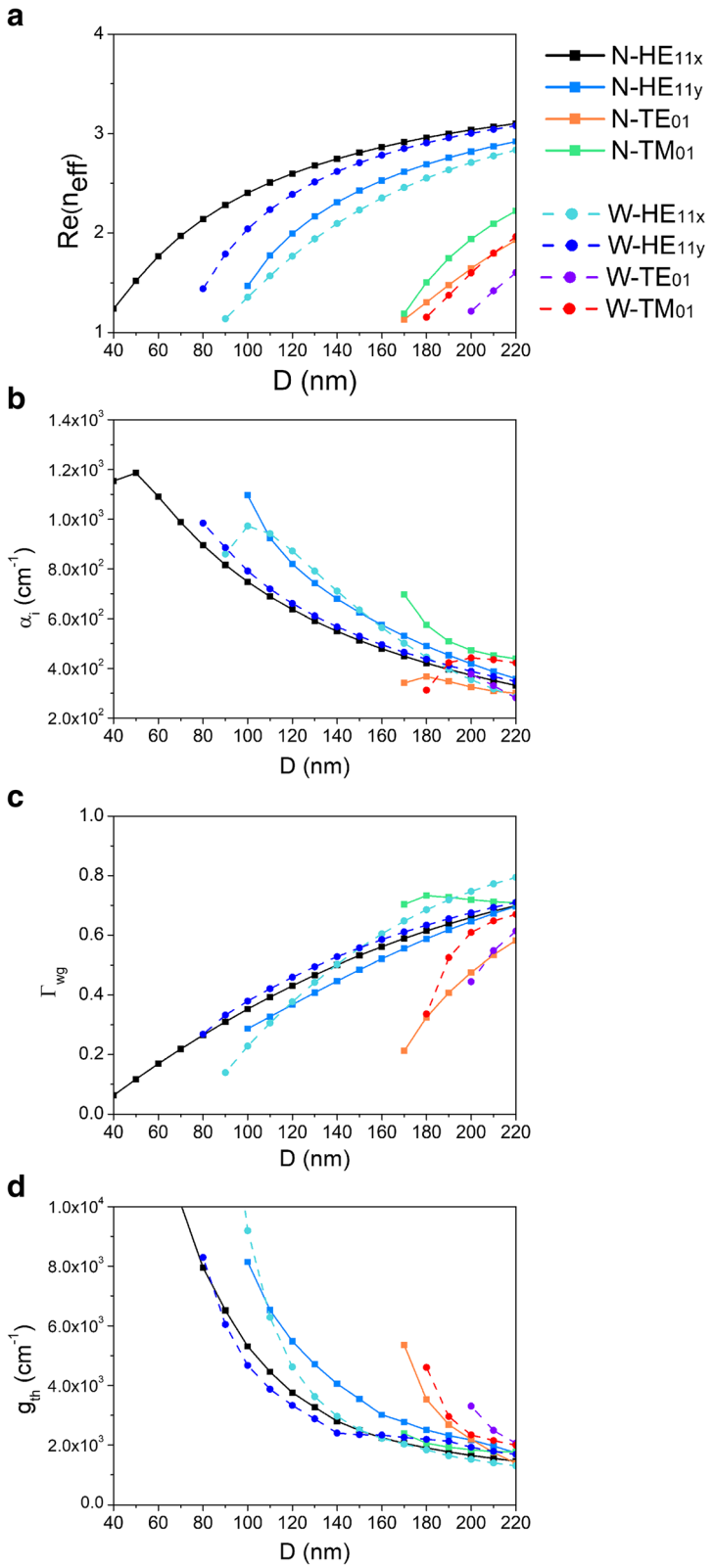

Fig. 4 Dependences of **a** the real part of the effective index, **b** modal loss, **c** modal confinement factor, and **d** threshold gain on nanowire diameter D

TE_{01} of CPN-W laser first cuts off at 200 nm, then mode TM_{01} of CPN-W laser cuts off at 180 nm, and modes TE_{01} and TM_{01} of CPN-N laser both cut off at 170 nm, whereas, the fundamental modes HE_{11x} and HE_{11y} have smaller cut-off diameters. Due to the asymmetric structure of CPN lasers, the fundamental mode no longer degenerates. Mode HE_{11x} has the smallest cut-off diameter of 40 nm during all the modes in a CPN-N laser. Mode HE_{11y} has the smallest cut-off diameter of 80 nm during all the modes in a CPN-W laser. In a CPN-N laser, $\mathrm{Re}(n_{\mathrm{eff}})$ of mode HE_{11x} is larger than that of mode HE_{11y}. Whereas, in a CPN-W laser, $\mathrm{Re}(n_{\mathrm{eff}})$ of mode HE_{11y} is larger than that of mode HE_{11x}, which results from the perpendicular component of the fundamental mode. Normally, the directions of electric field of HE_{11x} and TE_{01} are perpendicular to HE_{11y} and TM_{01}, respectively. In CPN-N and CPN-W lasers, the groove angles are 60° and 120°, resulting that *x*-component of modes dominate in CPN-N lasers and *y*-component of modes dominate in CPN-W lasers, as shown in Fig. 2d, e. Thus, modes HE_{11x} and TE_{01} have larger $\mathrm{Re}(n_{\mathrm{eff}})$ and smaller cut-off diameters in a CPN-N laser, whereas modes HE_{11y} and TM_{01} have larger $\mathrm{Re}(n_{\mathrm{eff}})$ and smaller cut-off diameter in a CPN-W laser.

The modal loss per unit length α_i and modal confinement factor Γ_{wg} are significant factors of the optical cavity relevant to lasing. The modal confinement factor is an indicator of how well the mode overlaps with the gain medium, which is defined as the ration between the modal gain the material gain in the active region [27, 28]. The modal loss per unit length α_i can be obtained from the imaginary part of modal propagation constant k_z as $\alpha_i = 2\,\mathrm{Im}[k_z]$. As shown in Fig. 4b, the modal loss of CPN-N and CPN-W lasers behaves negatively correlated with the nanowire diameter *D*. Whereas as shown in Fig. 4c, the confinement factor of CPN-N and CPN-W lasers behaves positively correlated with the nanowire diameter *D*. With the decreasing diameter of nanowire, the electromagnetic energy cannot be localized well inside the nanowire, more and more electromagnetic energy leaks. Part of electromagnetic energy scatters outside from the upper part of nanowire, and part of energy interacts with groove surface leading to more metal dissipation. It is interesting to note that mode TM_{01} in CPN-N laser has both relatively large confinement factor and modal loss. This can be attributed to the distribution of electric field of mode TM_{01}. As shown in Fig. 3d, electromagnetic energy distributes both inside the nanowire and around its surface. Though the confinement is tighter, the electromagnetic energy has stronger interaction with the metal groove. Importantly in Fig. 4c, as the nanowire diameter increases, the confinement factor becomes larger, indicating that the electromagnetic energy is confined in the cavity and overlaps well with the active region and potentially lower the lasing threshold.

Lasing threshold is the lowest excitation level at which laser output is dominated by stimulated emission rather than spontaneous emission. The threshold gain g_{th}, which describes the required gain per unit length for lasing, is defined as $g_{\mathrm{th}} = \frac{1}{\Gamma_{wg}}\left[\alpha_i + \frac{1}{L}\ln\left(\frac{1}{R}\right)\right]$, where *R* denotes the geometric mean of the reflectivity of the end facets of nanowire and *L* is the length of the nanowire F-P cavity [29]. The length *L* is fixed at 10 μm, which fits the experimental data in Ref. [12]. It needs to be noted that the nanowire here is the same as Ref. [11, 12], in which grown method of Au-particle catalyst was adopted. So, there is a gold cap on the top of nanowire. For the end facet with a gold cap, the reflectivity is larger than the other end facet, reaching around and more than 70%. We depict dependence of threshold gain g_{th} on *D* in Fig. 4d. It is obvious that the threshold gain decreases with the increasing nanowire diameter. This accords with the behaviors of modal loss and confinement factor, which are key factors of threshold gain. As the nanowire diameter increases, the electromagnetic energy is confined better inside the nanowire, leading to larger confinement factor and smaller energy leakage loss. Thus, the threshold gain becomes lower. In smaller diameter range, the threshold gain of mode HE_{11x} is lower than mode HE_{11y} in CPN-N laser, the threshold gain of mode HE_{11y} is lower than mode HE_{11x} in CPN-W laser. This also proves the mode HE_{11x} and HE_{11y} revolves in CPN lasers, due to the effect of groove angles on the electric field components.

Quality factor *Q* of a cavity mode is indicative of how long the stored energy of that mode remains in the cavity when interband transitions are absent, which is related to the photon lifetime τ_p enters the rate equation via the resonance frequency ω of the mode. For a F-P cavity, the quality factor is defined in the methods section [30]. High quality factor indicates a low rate of energy loss relative to the stored energy of the cavity and the oscillations die out slowly. So, the device can lase at a lower threshold and hence pump power could be reduced. We depict *Q* factor as functions of *D* in Fig. 5a. There are positive correlations between quality factors of all modes and diameter *D*, except for modes TM_{01} in CPN-N and CPN-W lasers. This could be attributed to the electric field distribution of mode TM_{01}, which has been discussed in the above. Furthermore, spontaneous emission rate in a nanolaser like CPN laser partly depends on environment of a light source. According to Fermi's golden role, the spontaneous emission rate of an emitter is proportional to the local density of optical states (LDOS) [31]. In an environment that structure is at the scale of the wavelength, the LDOS can be spatially controlled [32]. As a result, the LDOS of an emitter can be locally increased together with the rate

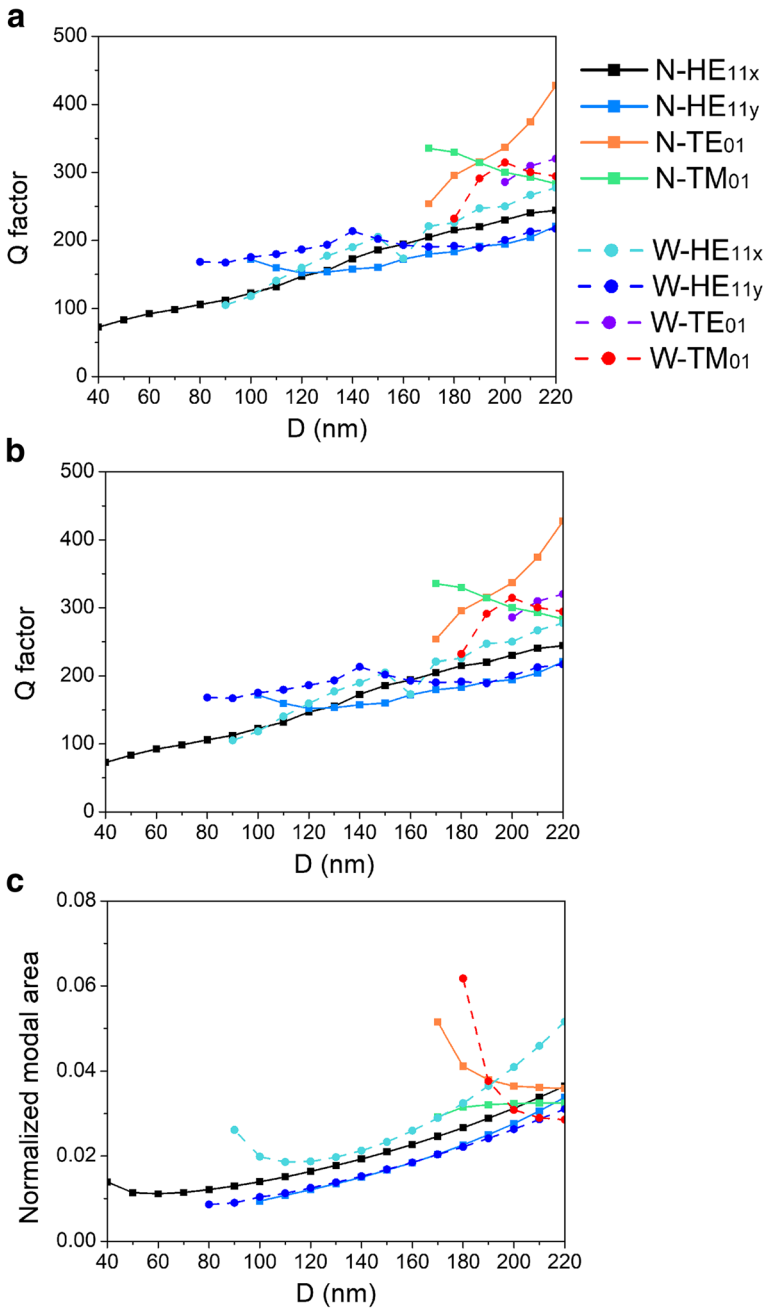

Fig. 5 Dependences of **a** quality factor, **b** Purcell factor, and **c** normalized modal area on nanowire diameter *D*

of spontaneous emission or decreased by the subwavelength microcavity, which is called the Purcell effect [33]. The nanolocalized electromagnetic energy can decrease the lasing threshold by enhancing the spontaneous emission rate via the Purcell effect. In CPN-N and CPN-W lasers, electromagnetic energy is tightly localized at subwavelength scale, resulting in large Purcell factors as shown in Fig. 5b. The metal groove modifies the dielectric environment around the nanowire and constructs a subwavelength cavity, enabling an ultra-small volume and coupling between an exciton and a microcavity mode. With the decreasing diameter, the Purcell factor increases sharply and reaches more than 100. Moreover, a large LDOS can enhance not only the rate of spontaneous emission, but also stimulated emission process in the lasing action. Lasing action could be easier achieved because the nanolocalized electromagnetic field of the hybrid plasmonic mode not only makes the excitons in the nanolaser

diffuse rapidly towards areas of faster recombination improving the overlap between material gain and plasmonic mode but also stimulates excited-state particles to transfer energy into plasmons of the same frequency, phase, and polarization. To quantify the subwavelength localization scale, the normalized modal area calculated using method in Ref. [13] and presented in Fig. 5c. Compared to Fig. 5b, the Purcell factor is inversely proportional to the normalized modal area, which proves that the cavity at subwavelength scale increases the Purcell factor and therefore enhances the spontaneous emission rate.

Conclusions

We proposed a CPN laser structure based on semiconductor nanowire and metal V-groove together with an ultrathin layer of dielectric. With the presence of high-index nanowire, channel plasmons can exist in the grooves with relatively large angles forming hybrid channel plasmonic modes. The metal groove modifies the dielectric environment around the nanowire and constructs a subwavelength cavity enabling the enhancement of spontaneous emission rate. Guiding and lasing properties were investigated using finite elements method. The fundamental mode HE_{11x} in CPN-N laser has a very small cut-off diameter, enabling ultra-small footprint of on-chip lasers. With the advantage of high confinement and ultra-small normalized modal area, the Purcell factor can reach more than 150 to greatly enhance the spontaneous emission rate. Besides, this CPN laser also has potential capability of integrating with plasmonic waveguides using CPP modes in V-groove plasmonic waveguides, which would find important applications in on-chip optical interconnections.

Methods/Experimental

Guiding and lasing properties were numerically calculated using finite elements method with the scattering boundary condition in the frequency, which is a commonly employed approach to mimic the necessary open boundary. The electric field distributions of the eigenmodes of CPN lasers are directly obtained by mode analyses. The guiding properties are calculated by the complex propagating constant with $\beta + i\alpha$. The real part of the modal effective index is calculated by $n_{\mathrm{eff}} = \mathrm{Re}(n_{\mathrm{eff}}) = \beta/k_0$, where k_0 is the vacuum wavevector. The effective mode area is calculated using [24]

$$A_m = \frac{W_m}{\max\{W(r)\}} = \frac{1}{\max\{W(r)\}} \iint_{\infty} W(r) d^2 r \quad (1)$$

where W_m is the total mode energy and $W(r)$ is the energy density (per unit length flowed along the direction of propagation). For dispersive and lossy materials, the $W(r)$ inside can be calculated using Eq. (2):

$$W(r) = \frac{1}{2}\left(\frac{d(\varepsilon(r)\omega)}{d\omega}|E(r)|^2 + \mu_0|H(r)|^2\right) \quad (2)$$

Quality factor and Purcell are defined as [30, 33]

$$\frac{1}{Q} = \frac{1}{\omega\tau_p} = \frac{v_{g,z}(\omega)}{\omega}\left[\alpha_i + \frac{1}{L}\ln\left(\frac{1}{R}\right)\right] \quad (3)$$

$$F_p = \frac{3}{4\pi^2}\left(\frac{\lambda}{n}\right)^3\left(\frac{Q}{V_{eff}}\right) \quad (4)$$

Equations to calculate modal loss, modal confinement factor, and threshold gain are provided in the main text; we do not narrate here again.

Abbreviations

CPN: Channel plasmon nanowire; CPN-N: Channel plasmon nanowire-narrow-angle; CPN-W: Channel plasmon nanowire-wide-angle; CPP: Channel plasmon-polariton

Funding

This work was supported by National Natural Science Foundation of China (61774021 and 61504010), the Fund of State Key Laboratory of Information Photonics and Optical Communications (Beijing University of Posts and Telecommunications), P. R. China (IPOC2017ZT02), and the Science and Technology program of Guangzhou Education Municipality (no. 1201630328).

Availability of Data and Materials

The dataset is available without restriction.

Authors' Contributions

WW proposed the structure of CPN laser, calculated properties of the proposed structure, and prepared the manuscript. XY, BS, JQ, and XZ analyzed the data and revised the manuscript. All authors read and approved the final manuscript.

Authors' Information

WW (associate professor) and JQ (associate professor) are from School of Mechanical and Electric Engineering, Guangzhou University, China.
XY (lecturer) and XZ (professor) are from State Key Laboratory of Information Photonics and Optical Communications, Beijing University of Posts and Telecommunications, Beijing 100,876, China.
BS (senior scientist) is from 4catalyzer Inc., 530 Old Whitfield St, Guilford 06437, CT, USA.

Competing Interests

The authors declare that they have no competing interests.

Publisher's Note

Author details

[1]School of Mechanical and Electric Engineering, Guangzhou University, Guangzhou 510006, China. [2]State Key Laboratory of Information Photonics and Optical Communications, Beijing University of Posts and Telecommunications, Beijing 100876, China. [3]4catalyzer Inc., 530 Old Whitfield St, Guilford, CT 06437, USA.

Received: 21 June 2018 Accepted: 24 July 2018
Published online: 31 July 2018

References

1. Panzauskie PJ, Yang P (2006) Nanowire photonics. Mater Today 9:36–45
2. Yan R, Gargas D, Yang P (2009) Nanowire photonics. Nature Photon 3:569–576

3. Hasan M, Huq MF, Mahmood ZH (2013) A review on electronic and optical properties of silicon nanowire and its different growth techniques. SpringerPlus 2:151
4. Couteau C, Larrue A, Wilhelm C, Soci C (2015) Nanowire lasers. Nanophotonics 4:90–107
5. Wu J, Ramsay A, Sanchez A, Zhang Y, Kim D, Brossard F, Hu X, Benamara M, Ware ME, Mazur YI, Salamo GJ, Aagesen M, Wang Z, Liu H (2016) Defect-free self-catalyzed GaAs/GaAsP nanowire quantum dots grown on silicon substrate. Nano Lett 16:504–511
6. Wang C, Hong Y, Ko Z, Su Y, Huang J (2017) Electrical and optical properties of au-catalyzed GaAs nanowires grown on Si (111) substrate by molecular beam epitaxy. Nanoscale Res Lett 12:290
7. Zimmler MA, Caspasso F, Müller S, Ronning C (2000) Optically pumped nanowire lasers: invited review. Semicond Sci Technol 25:024001
8. Versteegh MAM, Vanmaekelbergh D, Dijkhuis JI (2012) Room-temperature lasers emission of ZnO nanowires explained by many-body theory. Phys Rev Lett 108:157402
9. Gradečak S, Qian F, Li Y, Park HG, Lieber CM (2005) GaN nanowire lasers with low lasing thresholds. Appl Phys Lett 87:173111
10. Geburt S, Thielmann A, Röder R, Borschel C, McDonnell A, Kozlik M, Kühnel J, Sunter KA, Capasso F, Ronning C (2012) Low threshold room-temperature lasing of CdS nanowires. Nanotechnology 23:365204
11. Saxena D, Mokkapati S, Parkinson P, Jiang N, Gao Q, Tan HH, Jagadish C (2013) Optically pumped room-temperature GaAs nanowire lasers. Nat Photon 7:963–968
12. Wei W, Liu Y, Zhang X, Wang Z, Ren X (2014) Evanescent-wave pumped room-temperature single-mode GaAs/AlGaAs core-shell nanowire lasers. Appl Phys Lett 104:223103
13. Oulton RF, Sorger VJ, Zentgraf T, Ma RM, Gladden C, Dai L, Bartal G, Zhang X (2009) Plasmon lasers at deep subwavelength scale. Nature 461:629–632
14. Lu YJ, Kim J, Chen HY, Wu C, Dabidian N, Sanders CE, Wang CY, Lu MY, Li BH, Qiu S, Chang WH, Chen LJ, Shvets G, Shih CK, Gwo S (2012) Plasmonic nanolaser using epitaxially grown silver film. Science 337:450–453
15. Ho J, Tatebayashi J, Sergent S, Gong CF, Iwamoto S, Arakawa Y (2015) Low-threshold near-infrared GaAs-AlGaAs core-shell nanowire plasmon laser. ACS Photon 2:165–171
16. Bermúdez-Ureña E, Tutuncuoglu G, Cuerda J, Smith CLC, Bravo-Abad J, Bozhevolnyi SI, Fontcuberta i Morral A, García-Vidal FJ, Quidant R (2017) Plasmonic waveguide-integrated nanowire laser. Nano Lett 17:747–754
17. Novikov IV, Maradudin AA (2002) Channel polaritons. Phys Rev B 66:035403
18. Bozhevolnyi SI, Volkov VS, Devaux E, Ebbesen TW (2005) Channel plasmon-polariton guiding by subwavelength metal grooves. Phys Rev Lett 95:04682
19. Bian Y, Zheng Z, Zhao X, Liu L, Su Y, Liu J, Zhu J, Zhou T (2013) Hybrid plasmon polariton guiding with tight mode confinement in a V-shaped metal/dielectric groove. J Opt 15:055011
20. Bian Y, Zheng Z, Zhao X, Liu L, Su Y, Zhu J, Zhou T (2013) Modal properties of triangular metal groove/wedge based hybrid plasmonic structures for laser actions at deep-subwavelength scale. Opt Commun 297:102–108
21. Johnson P, Christy R (1972) Optical constants of the noble metals. Phys Rev B 6:4370–4379
22. Pile DFP, Gramotnev DK (2004) Channel plasmon-polariton in a triangular groove on a metal surface. Opt Lett 29:1069–1071
23. Gramotnev DK, Pile DFP (2004) Single-mode subwavelength waveguide with channel plasmon-polaritons in triangular grooves on a metal surface. Appl Phys Lett 85:6323
24. Oulton RF, Sorger VJ, Genov DA, Pile DFP, Zhang X (2008) A hybrid plasmonic waveguide for subwavelength confinement and long-range propagation. Nat Photon 2:496–500
25. Wei W, Zhang X, Ren X (2014) Asymmetric hybrid plasmonic waveguides with centimeter-scale propagation length under subwavelength confinement for photonic components. Nanoscale Res Lett 9:599
26. Cheng P, Chiang C, Chung Y, Tien C, Lin T (2014) Coupled nanowire-based hybrid plasmonic nanocavities on thin substrates. Nanoscale Res Lett 9:641
27. Visser TD, Blok HD, Demeulenaere B, Lenstra D (1997) Confinement factors and gain in optical amplifiers. IEEE J Quantum Electron 33:1763–1766
28. Maslov AV, Ning CZ (2004) Modal gain in a semiconductor nanowire laser with anisotropic bandstructure. IEEE J Quantum Electron 40:1389–1397
29. Yaris A (1975) Quantum Electronics. Wiley, New York
30. Chang SW, Lin TR, Chuang SL (2010) Theory of plasmonic Fabry-Perot nanolaser. Opt Express 18:15039–15053
31. Novotny L, Hecht B (2006) Principles of nano-optics. Cambridge Univ Press, Cambridge
32. Drexhage KH (1970) Influence of a dielectric interface on fluorescence decay time. J Lumin 1:693–701
33. Purcell EM (1995) Spontaneous emission probabilities at radio frequencies. Confined Electrons and Photons 340:839